TRPML3-mediated lysosomal Ca^{2+} release enhances drug sequestration and biogenesis, promoting osimertinib resistance in non-small cell lung cancer

MI SEONG KIM[1,2] and MIN SEUK KIM[1]

[1]Department of Oral Physiology, Institute of Biomaterial-Implant, School of Dentistry, Wonkwang University, Iksan, Jeonbuk 54538, Republic of Korea; [2]Wonkwang Dental Research Institute, School of Dentistry, Wonkwang University, Iksan, Jeonbuk 54538, Republic of Korea

Received May 9, 2025; Accepted July 1, 2025

DOI: 10.3892/or.2025.8946

Abstract. Lysosomes and lysosomal Ca^{2+} play crucial roles in cellular homeostasis and drug resistance. The lysosomal Ca^{2+} channel transient receptor potential mucolipin 3 (TRPML3; also known as mucolipin-3 or MCOLN3) is a key regulator of autophagy and membrane trafficking; however, its role in tyrosine kinase inhibitor (TKI) resistance remains unclear. The contribution of TRPML3 to osimertinib resistance in non-small cell lung cancer (NSCLC) was therefore assessed. Using publicly available RNA sequencing data, including profiles from clinical samples before and after osimertinib treatment, *TRPML3* expression was measured in lung adenocarcinoma (LUAD) tissues. Additionally, two-dimensional cell culture of, and three-dimensional spheroids derived from, NSCLC cell lines were used to elucidate roles of TRPML3 in drug resistance. *TRPML3* expression was significantly upregulated in both LUAD tissues from patients with residual disease after osimertinib treatment, as well as in osimertinib-resistant NSCLC cells. *TRPML3* knockdown in resistant PC9 cells restored sensitivity to osimertinib and multiple TKIs; this was replicated in spheroid models. Mechanistically, osimertinib induced intracellular Ca^{2+} oscillations in PC9 cells via lysosomal Ca^{2+} release through TRPML3 rather than through TRPML1. In summary, the present findings suggest that elevated TRPML3 expression compensates for TRPML1 to maintain lysosomal acidity and biogenesis during TKI treatment, facilitating drug sequestration and resistance and identifying *TRPML3* as a potential target for overcoming osimertinib resistance in NSCLC.

Correspondence to: Professor Min Seuk Kim, Department of Oral Physiology, Institute of Biomaterial-Implant, School of Dentistry, Wonkwang University, Iksandaero 460, Iksan, Jeonbuk 54538, Republic of Korea
E-mail: happy1487@wku.ac.kr

Abbreviations: TKI, tyrosine kinase inhibitor; NSCLC, non-small cell lung cancer; LUAD, lung adenocarcinoma; TFEB, transcription factor EB; FBS fetal bovine serum; TRPMLs, transient receptor potential mucolipins; MLIV, type IV mucolipidosis; RNA-seq, RNA-sequencing; RT-qPCR, reverse transcription-quantitative PCR

Key words: osimertinib, *TRPML3,* NSCLC, drug resistance, lysosome, Ca^{2+} signaling

Introduction

Lysosomes, often referred to as the digestive units of the cells, are membrane-bound organelles essential for recycling damaged intracellular components and organelles. In addition to their degradative functions, lysosomes play key roles in multiple physiological and pathological processes (1), including nutrient sensing, metabolic regulation and aging. They have emerged as critical mediators of drug resistance, particularly in cancer treatment with tyrosine kinase inhibitors (TKIs) (2,3). The acidic environment within lysosomes, coupled with the cytosolic pH gradient, facilitates the passive uptake of hydrophobic, weakly basic drugs such as TKIs. This pH-dependent sequestration reduces TKI efficacy by trapping within lysosomes (4-6). Cancer cells with increased drug sequestration have been shown to exhibit heightened resistance to therapy, suggesting that lysosomal trapping is a major therapeutic barrier to treatment success (3,6). However, the mechanisms by which cells tolerate high TKI concentrations within lysosomes remain poorly understood.

Lysosomes are as crucial intracellular Ca^{2+} stores, releasing Ca^{2+} to regulate signaling pathways essential for organelle homeostasis and acidification (7). Ca^{2+} channels, including transient receptor potential mucolipins (TRPMLs) and two-pore channels located on the endolysosomal membrane, are essential for proliferation, migration and calcium homeostasis, all of which are significant both normal physiology and disease (8). The TRPML family, also known as mucolipins, consists of three isoforms, TRPML1, -2 and -3, each functioning as inward-rectifying cation channels with physiological and pathological roles (9). TRPML1, the first identified isoform, has been linked to type IV mucolipidosis (MLIV), a disorder caused by loss-of-function mutations (10). It is activated by phosphatidylinositol-3,5-bisphosphate, voltage changes and low luminal pH (11). As a non-selective cation channel,

it facilitates lysosomal degradation. Its deficiency leads to excessively acidic lysosomes due to impaired H^+ efflux (12). Fibroblasts from patients with MLIV exhibit defective lysosomal degradation of macromolecules (13). TRPML1 regulates autophagy by releasing Ca^{2+}, which is necessary for mTORC1 modulation and autophagosome-lysosome fusion (14). Finally, it promotes lysosomal biogenesis by releasing Ca^{2+}, which triggers transcription factor EB (TFEB) dephosphorylation and nuclear translocation (15).

TRPML3 also plays a key role in endocytic and autophagic pathways (16). As a phosphatidylinositol-3-phosphate effector, it facilitates Ca^{2+} release into the cytoplasm, a process essential for membrane fusion and autophagosome formation (17). Despite their functional overlap, TRPML1 and TRPML3 differ in pH sensitivity: The latter is fully active at a higher pH (~6.3), whereas the former operates optimally at a lower pH (~4-5.5) (18). Neutralizing lysosomal pH with uropathogenic *E. coli* has been shown to activate TRPML3, triggering Ca^{2+} release and lysosomal exocytosis (19). Reduced luminal Ca^{2+} in early endosomes has been linked to increased acidification (20), while Ca^{2+} release through TRPML3 supports H^+ uptake via the vacuolar H^+ pump, helping maintain lysosomal acidity (21). These findings suggest the hypothesis that TRPML3 enhances lysosomal TKI sequestration, contributing to acquired drug resistance. This hypothesis warrants further investigation.

In the present study, TRPML3 expression in non-small cell lung cancer (NSCLC) tissues during the development of drug resistance was initially determined. Using two- and three-dimensional (2D and 3D, respectively) cell-culture models, TRPML3 function in the regulation of lysosomal pH, biogenesis and drug resistance was investigated. It was found that TRPML3 enhances lysosomal sequestration of osimertinib and compensates for TRPML1 in lysosomal biogenesis during treatment, significantly contributing to drug resistance.

Materials and methods

Cell culture, reagents and transfection. Human PC9 and HCC827 NSCLC cell lines were generously provided by Dr Jin Kyung Rho (Asan Medical Center, Ulsan University). The cells were cultured in RPMI-1640 medium (HyClone; Cytiva) supplemented with 10% fetal bovine serum (FBS) and antibiotics (100 U/ml penicillin and 100 μg/ml streptomycin) in a humidified incubator with 5% CO_2. All cell lines used in the present study were authenticated by short tandem repeat profiling (KOMA Biotech, Inc.) and were routinely screened for microbial contamination as part of standard quality control procedures. The TRPML3-GCaMP6 construct, generated by inserting the full-length GCaMP6 sequence into the p3XFLAG-CMV-7.1-TRPML3 vector (17), was kindly provided by Dr Hyun Jin Kim (Sungkyunkwan University). The pCMV-TRPML3 expression vector containing wild-type TRPML3 (NM_018298) was obtained from OriGene Technologies, Inc. Reagents and their sources were as follows: osimertinib (Selleck Chemicals), Cell Fractionation Kit (Cell Signaling Technology, Inc.), anti-TFEB (cat. no. 4240s), anti-Nanog (cat. no. 3580s; both from Cell Signalling Technology, Inc.), TRPML agonist ML-SA1 (MilliporeSigma; cat. no. SML0627), TRPML inhibitor ML-SI1 (GlpBio; cat. no. GC19764), anti-Myc (cat. no. sc-40; Santa Cruz Biotechnology, Inc.), anti-CD44 (cat. no. MA5-13890; Thermo Fisher Scientific, Inc.), anti-CD133 (cat. no. ab16048), anti-lamin-B1 (cat. no. ab19898; both from Abcam), anti-TRPML1 (cat. no. MBS9205163; MyBioSource, Inc.), anti-TRPML3 (cat. no. 13879-1-AP; Proteintech Group, Inc.) and anti-GAPDH (cat. no. bs2188R; BIOSS). For transient gene silencing, synthetic small interfering RNAs (siRNAs) targeting *TRPML3* and scrambled control siRNAs were purchased from Integrated DNA Technologies, Inc. Their sequences were as follows: *TRPML3* siRNA sense, 5'-GUAGAAUUUACCUCUACUCAUUCAT-3' and antisense, 3'-AUCAUCUUAAAUGGAGAUGAGUAAGUA-5'; scrambled siRNA sense, 5'-CGUUAAUCGCGUAUAAUACGCUAT-3' and antisense, 3'-AUACGCGUAUUAUACGCGAUUAACGAC-5'. The siRNAs and expression vectors were introduced using Lipofectamine RNAiMAX and Lipofectamine 3000, respectively, according to the manufacturer's protocols (Thermo Fisher Scientific, Inc.). In brief, each mixture of siRNA (30 nM per 35-mm dish) with RNAiMAX and expression vectors (2.5 μg per 35-mm dish) with Lipofectamine 3000 was incubated for 5 min and 15 min, respectively, at 24˚C. Each sample was then subjected to subsequent experiment following an additional incubation of 72 and 24 h, respectively. To generate a stable TRPML3 knockout cell line, an sgRNA targeting TRPML3 (RefSeq NM_018298.11) was designed and synthesized by Macrogen, Inc. (5'-CAGCTACTCACAACTACCTCAGG-3'). It was inserted into the pSp-U6-Cas9-2A-Puro plasmid; cells were transfected with either the TRPML3-specific construct or the empty vector control. After puromycin selection (2-10 μg/ml) for two weeks, the TRPML3 knockout was confirmed using western blotting.

Osimertinib-resistant NSCLC sub-cell lines. Resistant sub-lines of PC9 and HCC827, designated as PC9/OR and HCC827/OR, respectively, were generated by gradually increasing osimertinib concentrations ($1x10^{-4}$, $1x10^{-3}$, $1x10^{-2}$, and $1x10^{-1}$ μM) over five months. Surviving cells were cultured in $1x10^{-1}$ μM osimertinib for an additional month to confirm the stability of resistance. Viability at each subculture step was assessed using 3-[4,5-dimethylthiazol-2-yl]-2,5 diphenyl tetrazolium bromide (MTT) assays.

Collection and analysis of publicly available RNA sequencing (RNA-Seq) data. To measure gene expression changes in lung adenocarcinoma (LUAD) tissues during the development of osimertinib resistance, a publicly available RNA-seq dataset (GSE253742) from the Gene Expression Omnibus (GEO) database (https://www.ncbi.nlm.nih.gov/geo/) was analyzed, representing paired LUAD tumor samples collected before and after osimertinib treatment (22). Data were processed using Expression Differential Expression Gene Analysis (ExDEGA v5.1.1.1) software (Ebiogen Inc.). Briefly, raw data were subjected to quality control with FastQC, followed by adapter trimming and low-quality read removal using Fastp (23). Processed reads were aligned to the reference genome with STAR (24), and quantified using Salmon (25). Read count normalization was performed using the TMM + CPM method in EdgeR (26). Data mining and visualization were performed

using ExDEGA and Multi Experiment Viewer (MeV 4.9.0; http://www.tm4.org) (27).

Reverse transcription-quantitative PCR (RT-qPCR). Total RNA was isolated from cell lines using TRIzol® reagent (Invitrogen; Thermo Fisher Scientific, Inc.), following the manufacturer's protocol. Subsequently, 1 μg of RNA was converted into cDNA using the High-Capacity RNA-to-cDNA kit (Applied Biosystems; Thermo Fisher Scientific, Inc.), following the manufacturer's protocol. Quantitative PCR (qPCR) was conducted using VeriQuest SYBR Green qPCR Master Mix (Affymetrix; Thermo Fisher Scientific, Inc.) on an ABI PRISM 7900 Sequence Detection System (Applied Biosystems; Thermo Fisher Scientific, Inc.). The thermal cycling conditions were as follows: initial denaturation at 95˚C for 20 sec, followed by 40 cycles of denaturation at 95˚C for 3 sec and annealing/extension at 60˚C for 30 sec. Primers were as follows: *TRPML3* forward, 5'-TCCGTTGGGAAT CATGCTTAT-3' and reverse, 5'-AGTGCTGACAGATTG CCATAGC-3'; *GAPDH* forward, 5'-ATGGAAATCCCATCA CCATCTT-3' and reverse, 5'-CGCCCCACTTGATTTTGG-3'. *GAPDH* expression was used to normalize data and controls for variations in mRNA concentration. Expression levels were calculated using the $2^{-\Delta\Delta Cq}$ method (28).

Generation of cancer cell line-derived spheroid. To generate 3D spheroid cultures, cells were resuspended in culture medium supplemented with threefold the standard FBS concentration at a density of $6x10^4$ cells/ml for PC9 and its subline and $4.2x10^4$ cells/ml for HCC827 and its subline. Cell suspensions were mixed with VitroGel Hydrogel Matrix (Well Bioscience Inc.; http://www.thewellbio.com) at a 2:1 (v/v) ratio; the 50 μl of the mixture was added per well in U-bottom 96-well plates (S-bio Sumitomo Bakelite Co., Ltd.). Plates were centrifuged at 1,000 x g for 5 min at 24˚C, and 200 μl of regular culture medium was added per well. Aggregates were incubated in the hydrogel matrix at 37˚C in a 5% CO_2 atmosphere for three days to form multilayered spheroids. These spheroids were treated with osimertinib or left untreated (DMSO vehicle only) for an additional 9 days, with medium refreshed every 3 days. Spheroids were imaged using a NIKON Eclipse TS100 microscope equipped with an FL-20BW CMOS camera (Tucsen Photonics Co., Ltd.). Images were captured with Mosaic 2.4 software (Tucsen Photonics Co., Ltd.) and analyzed using ImageJ software (version 1.51k; National Institutes of Health) to measure spheroid diameters and other parameters. Viability was measured using the Cell Counting Kit-8 (CCK-8) assay kit (Dojindo Laboratories, Inc.), according to the manufacturer's protocol. In brief, 20 μl of CCK-8 solution was added to each well and incubated at 37˚C for 1 h, after which the absorbance was measured at 450 nm using an iMark microplate reader (Bio-Rad Laboratories, Inc.).

Western blot analysis. Western blotting was performed using established methods (29). Cell lysates prepared in RIPA buffer (Invitrogen; Thermo Fisher Scientific, Inc.) were sonicated for 5 sec at 50% amplitude and incubated on ice for 10 min. Debris was pelleted at 14,440 x g for 10 min at 4˚C. Supernatant protein concentrations were quantified using the BCA assay. Equal amounts of protein (20 μg per sample) were separated using 8% SDS-PAGE, followed by transfer to 0.2-μm polyvinylidene difluoride membranes (Cytiva). The membrane was blocked with 5% bovine serum albumin (GenDEPOT, LLC) in Tris-buffered saline with 0.1% Tween 20 at 4˚C for 2 h. Primary antibodies against TRPML1, TRPML3, TFEB, lamin-B1, Myc, CD44, CD133, Nanog and GAPDH were used at a 1:1,000 dilution. The membranes were incubated overnight at 4˚C with the primary antibodies, followed by incubation with horseradish peroxidase (HRP)-linked secondary IgG antibody (1:2,500; Santa Cruz Biotechnology, Inc.; cat. no. sc-516102 for anti-mouse, and cat. no. sc-2357 for anti-rabbit) for 2 h at 4˚C. Protein bands were visualized and quantified using the AzureSpot 2.0 software (Azure Biosystems, Inc.). Whole-cell lysate from spheroids cultured in VitroGel Hydrogel Matrix (Well Bioscience, Inc.) were extracted using VitroGel Organoid Recovery Solution (Well Bioscience, Inc.) according to the manufacturer's protocol. Briefly, spheroids were transferred to 1.5-ml tubes, washed with PBS, and resuspended in 1 ml of pre-warmed (37˚C) VitroGel Organoid Recovery Solution. The solution was gently pipetted to isolate the spheroids, followed by a brief incubation at 37˚C. After centrifugation at 100 x g for 5 min, pellets were collected and lysed in RIPA buffer. To measure TFEB translocation from the cytoplasm to the nucleus, cytosolic and nuclear fractions were isolated using a Cell Fractionation Kit (Cell Signaling Technology, Inc.), following the manufacturer's instructions. Briefly, cell pellets were resuspended in Cytoplasm Isolation Buffer and incubated at 4˚C for 5 min. Suspensions were centrifuged at 500 x g for 5 min at 4˚C, and cytosolic supernatants were collected. Nuclear pellets were resuspended in Membrane Isolation Buffer, re-pelleted at 8,000 x g for 5 min at 4˚C, and resuspended in Cytoskeleton/Nuclear Isolation Buffer. Both fractions were analyzed using western blotting.

Cell cycle analysis. Cells were seeded at a density of $7x10^5$ per 60 mm culture dish. Following incubation under the designated conditions, they were detached using 0.05% Trypsin-EDTA (Gibco; Thermo Fisher Scientific, Inc.) and fixed in 70% ethanol at -20˚C for 2 h, then stained with 0.5 ml of propidium iodide/RNase staining buffer (BD Biosciences) for 15 min. Flow cytometry was performed on at least 20,000 cells using a FACScan analyzer (BD CellQuest™ Pro version 5.2; BD Biosciences).

MTT assay. Cell viability was assessed using the Viability Assay Kit (Cellrix; MediFab) following the manufacturer's protocol. Cells were seeded at a density of $1x10^4$ per well in 96-well plates, treated with 10 μl of assay reagent containing water-soluble tetrazolium salt, and incubated at 37˚C for 30 min. The production of water-soluble formazan was evaluated by measuring the absorbance at 450 nm using an iMark microplate reader (Bio-Rad Laboratories, Inc.).

Imaging of intracellular Ca^{2+} ($Ca^{2+}{}_i$) and green fluorescent protein (GFP). Intracellular Ca^{2+} levels were measured by incubation with Fura-2/AM (MilliporeSigma) at 37˚C for 50 min, followed by perfusion with a HEPES-buffered solution containing 140 mmol/l NaCl, 5 mmol/l KCl, 1 mmol/l $MgCl_2$, 1 mmol/l $CaCl_2$, 10 mmol/l HEPES, and 10 mmol/l glucose, adjusted to pH 7.4 and 310 mOsm. For Ca^{2+}-free conditions,

the $CaCl_2$ was replaced with 1 mmol/l EGTA. Osimertinib and other compounds, including ML-SI1 and MS-SA1, were diluted in a Ca^{2+}-free HEPES buffer. Fluorescence excitation was performed at 340 and 380 nm, with emission at 510 nm-captured using an sCMOS camera (Andor Technology Ltd.). Ratio-metric data (F_{340}/F_{380}) were analyzed using Meta-Fluor Fluorescence Ratio Imaging software (Molecular Devices, LLC). GCaMP6 fluorescence intensities were measured at an excitation wavelength of 488 nm, with emission at 510 nm measured using an sCMOS camera (Andor Technology Ltd.) and analyzed using Meta-Fluor Fluorescence Ratio Imaging software (Molecular Devices, LLC).

Measurement of lysosomal pH. Lysosomal pH was measured using a LysoSensor Yellow/Blue DND-160 (Thermo Fisher Scientific, Inc.), according to the manufacturer's protocol. Cells cultured in 35 mm confocal dishes (SPL Life Sciences) were incubated with the dye for 10 min at 37˚C. After a brief wash with HEPES buffer, cells were continuously exposed to osimertinib diluted in HEPES buffer. Fluorescent images were captured using an sCMOS camera (Andor Technology Ltd.) with excitation at 329 and 384 nm and emission at 440 and 540 nm, respectively. Data were analyzed using MetaMorph software (Molecular Devices, LLC), and lysosomal pH was determined by calculating the fluorescence intensity ratio of 384 nm (yellow, acidic) to 329 nm (blue, less acidic), with fold changes expressed relative to the control (scr-cells pre-osimertinib treatment).

Measurement of lysosomal area in a single cell. The lysosomal area in individual cells was measured using LysoTracker Red DND-99 (Thermo Fisher Scientific, Inc.), according to the manufacturer's instructions. Cells were plated in 35 mm confocal dishes and transfected with either siML3 or scrambled RNA as a control. After 72 h, the cells were treated with 0.01 μM osimertinib, incubated for 24 h, and stained with LysoTracker Red DND-99 for 30 min. Fluorescence was excited at 577 nm and emitted at 590 nm, and images were captured using a confocal microscope (FV1000; Olympus Corporation). Image analysis was performed using ImageJ software (version 1.52v; National Institutes of Health).

Statistical analysis. Data were analyzed using Origin 2020 software (OriginLab Corporation). Results are presented as the mean ± standard deviation (SD) based on a minimum of three independent experiments. Statistical significance was evaluated using one-way analysis of variance (ANOVA), followed by Tukey's post-hoc test for multiple comparisons. $P<0.05$ was considered to indicate a statistically significant difference.

Results

Endogenous TRPML3 expression is upregulated in osimertinib-residual LUAD tumor tissues and osimertinib-resistant NSCLC cell lines. To identify genes involved in osimertinib-induced lysosomal pH dysregulation, the GEO dataset GSE253742 was analyzed, which includes RNA-seq data from eight clinical LUAD specimens (four naive tumors and four osimertinib-residual tumors). Of the 40,929 genes analyzed, *TRPML3* was the only gene whose expression was significantly increased (5.121±0.045; |fold change|≥2, log2 ≤3, $P<0.05$) in osimertinib-residual tumors within a subset of 26 genes related to lysosomal acidification (GO:0007042) (Fig. 1A). Based on these findings, the expression was next measured in NSCLC cell lines, specifically PC9 and HCC827, and in their osimertinib-resistant sublines. *TRPML3* mRNA levels were significantly higher in osimertinib-resistant cells than in their parental lines (Fig. 1B). Additionally, osimertinib exposure and resistance increased TRPML3 protein expression, whereas TRPML1 expression remained unchanged regardless of treatment or resistance (Fig. 1C and D). These findings suggest that TRPML3 plays a critical role in the lysosomal response associated with osimertinib resistance in NSCLC.

TRPML3 knockdown reduces multi-drug tolerance in osimertinib-resistant PC9 cells. siRNA-mediated *TRPML3* knockdown (siML3) was next performed in PC9 cells and their osimertinib-resistant subline PC9/OR. TRPML3 expression was efficiently reduced without affecting TRPML1 expression (Fig. 2A). Next, the effects of TRPML3 depletion on osimertinib-induced G0/G1 cell-cycle arrest was examined. Cells transfected with siML3 or scrambled RNA (control) were incubated for 48 h with or without 0.01 μM osimertinib. In PC9 cells, *TRPML3* knockdown did not alter osimertinib-induced G0/G1 arrest but increased the sub-G0 population (Fig. 2B), suggesting increased cell death. By contrast, *TRPML3* knockdown in PC9/OR cells restored their sensitivity to osimertinib-induced G0/G1 arrest (Fig. 2C). All tested TKIs, including osimertinib (Fig. 2D), lapatinib (Fig. 2E), gefitinib (Fig. 2F) and erlotinib (Fig. 2G), reduced PC9 viability in a dose-dependent manner. By contrast, PC9/OR cells displayed cross-resistance to all TKIs except for lapatinib. Finally, *TRPML3* knockdown restored the sensitivity to osimertinib and other TKIs in these resistant cells. These findings indicate that TRPML3 plays a critical role in mediating TKI resistance in NSCLC cells.

TRPML3 modulates osimertinib sensitivity and growth in spheroids. To better mimic tumors *in vivo*, 3D spheroids derived from *TRPML3*-overexpressing and -silenced cells treated with osimertinib treatment for 9 days were employed. was initiated on day 0 and maintained for 9 days. Spheroid viability and size were assessed using CCK-8 assays and bright-field imaging, respectively (Fig. 3A). Western blotting confirmed changes in TRPML3 expression without affecting TRPML1 expression (Fig. 3B). Blotting with antibodies against the myc tag and TRPML3 verified pCMV-TRPML3 expression in PC9 and HCC827 cells, whereas targeting TRPML3 with sgRNA reduced endogenous TRPML3 expression in PC9/OR and HCC827/OR cells. On day 0, increased expression of the spheroid markers CD44, CD133 and Nanog was observed in spheroids, but not in parental 2D cultures (Fig. 3C and D). TRPML3 modulation did not affect spheroid formation. Next, the effects of TRPML3 overexpression (Fig. 3E and F) and silencing (Fig. 3G and H) on osimertinib-induced toxicity were assessed in spheroids derived from osimertinib-sensitive (PC9 and HCC827) and -resistant (PC9/OR and HCC827/OR) cells. Osimertinib produced a dose-dependent decrease in spheroid viability in sensitive cell-derived spheroids (Fig. 3E and F), whereas those derived from resistant cells exhibited greater

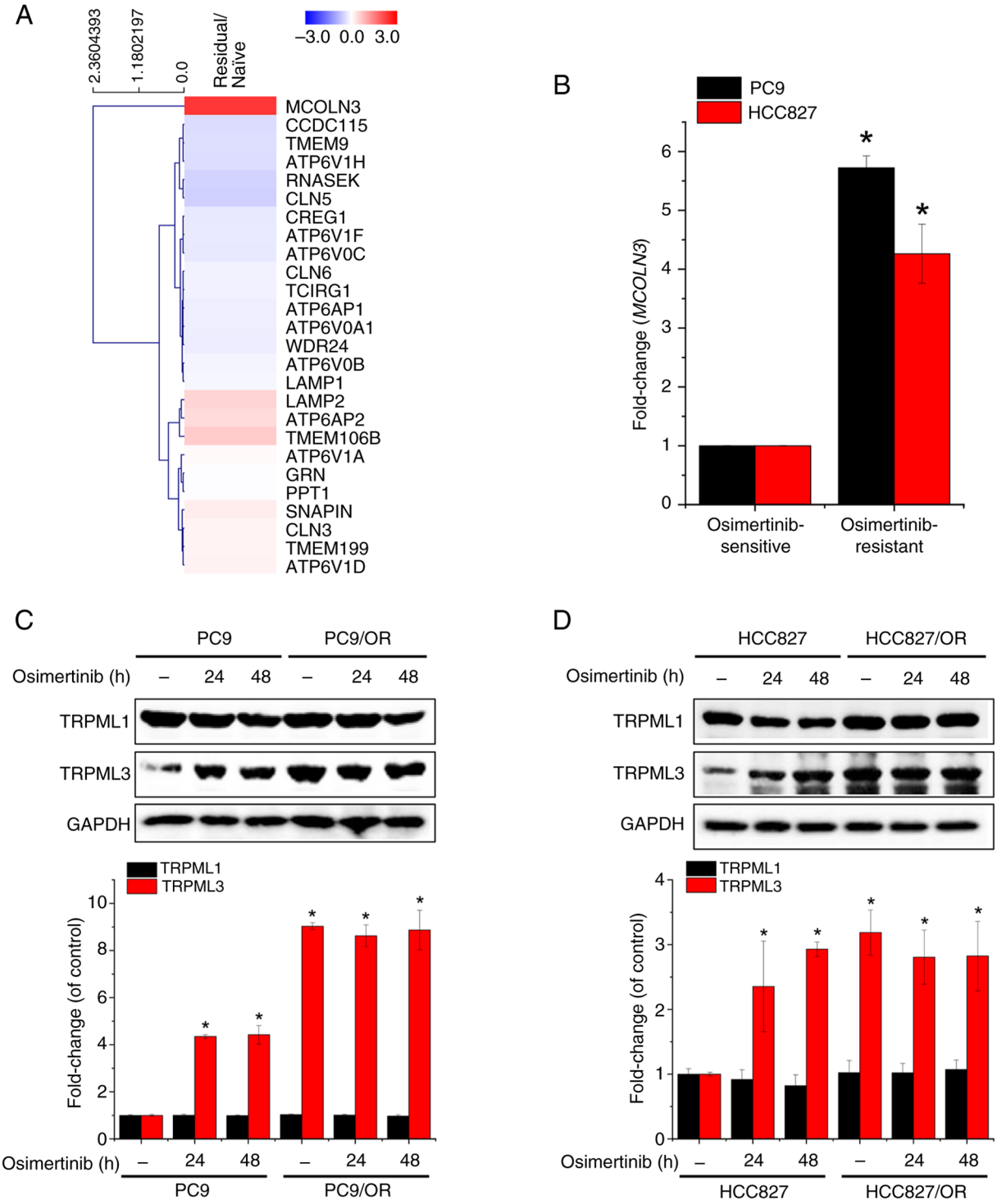

Figure 1. Differential gene and protein expression in osimertinib-residual LUAD tissues and TRPML3 levels in osimertinib-sensitive and -resistant non-small cell lung cancer cells. (A) Heatmap of differentially expressed genes in residual vs. naive LUAD tissues (both n=4) generated using hierarchical clustering with Euclidean distance. Color intensities indicate changes in average normalized expression levels. (B) *TRPML3* mRNA expression in PC9 and HCC827, cells and their osimertinib-resistant sublines. Data are shown as fold-changes relative to osimertinib-sensitive controls (n=3). (C and D) Protein levels of TRPML1 and TRPML3 in (C) PC9 and PC9/OR, and (D) HCC827 and HCC827/OR cells, treated with 0.01 μM osimertinib. GAPDH served as a loading control. Statistical analysis (lower panels) is presented as fold-change relative to DMSO-treated controls (n=3). *P<0.05. LUAD, lung adenocarcinoma; TRPML, transient receptor potential mucolipin.

tolerance (Fig. 3G and H). TRPML3 overexpression in PC9 (ML3 OE-PC9) and HCC827 (ML3 OE-HCC827) spheroids attenuated osimertinib-induced viability reductions at 0.1 μM (PC9) and 1 μM (HCC827). Conversely, TRPML3 silencing significantly reduced osimertinib tolerance in spheroids derived from PC9/OR and HCC827/OR cells (Fig. 3G and H). Consistent with these findings, intracellular TRPML3 levels influenced osimertinib-induced reductions in spheroid size. Spheroids were treated with osimertinib at the induced concentrations; bright-field images were captured

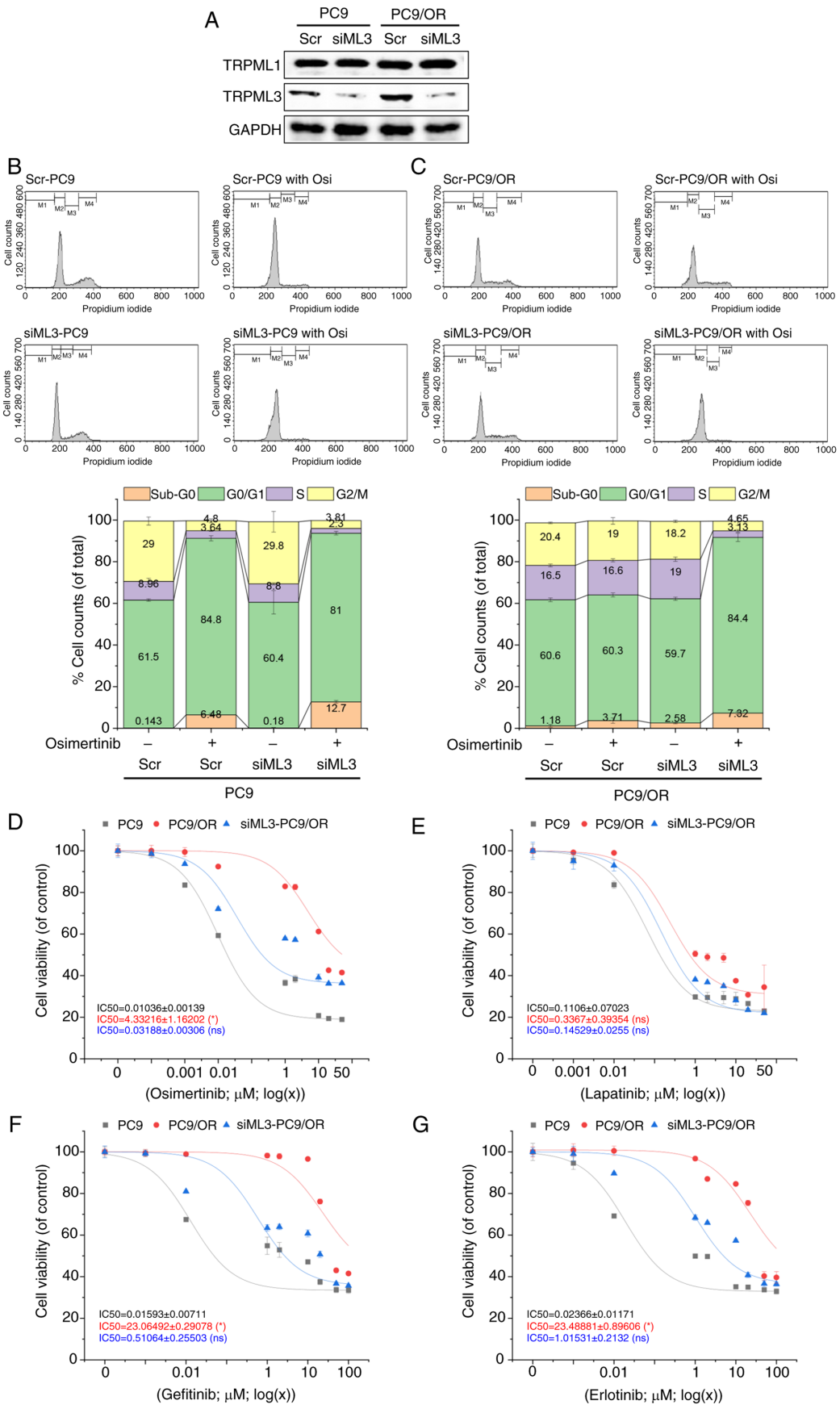

Figure 2. TRPML3 deletion restores sensitivity to osimertinib-induced cell-cycle arrest and death in PC9/OR cells. (A) Confirmation of TRPML3 siRNA knockdown in PC9 and PC9/OR cells, with no effect on TRPML1 expression. GAPDH was used for normalization. (B and C) Cell-cycle phase distributions in (B) PC9 and (C) PC9/OR cells transfected with siML3 or scrambled RNA (scr), then treated with 0.01 μM osimertinib for 48 h. Flow cytometric data are presented as percentages of cells per phase ($2x10^4$ cells per sample, n=4). (D-G) Viability of PC9, PC9/OR and siML3-PC9/OR cells treated with increasing concentrations of (D) osimertinib, (E) lapatinib, (F) gefitinib, or (G) erlotinib for 72 h, assessed by MTT assay. Data show percentages relative to DMSO-treated controls (n=3). TRPML, transient receptor potential mucolipin; si-, small interfering.

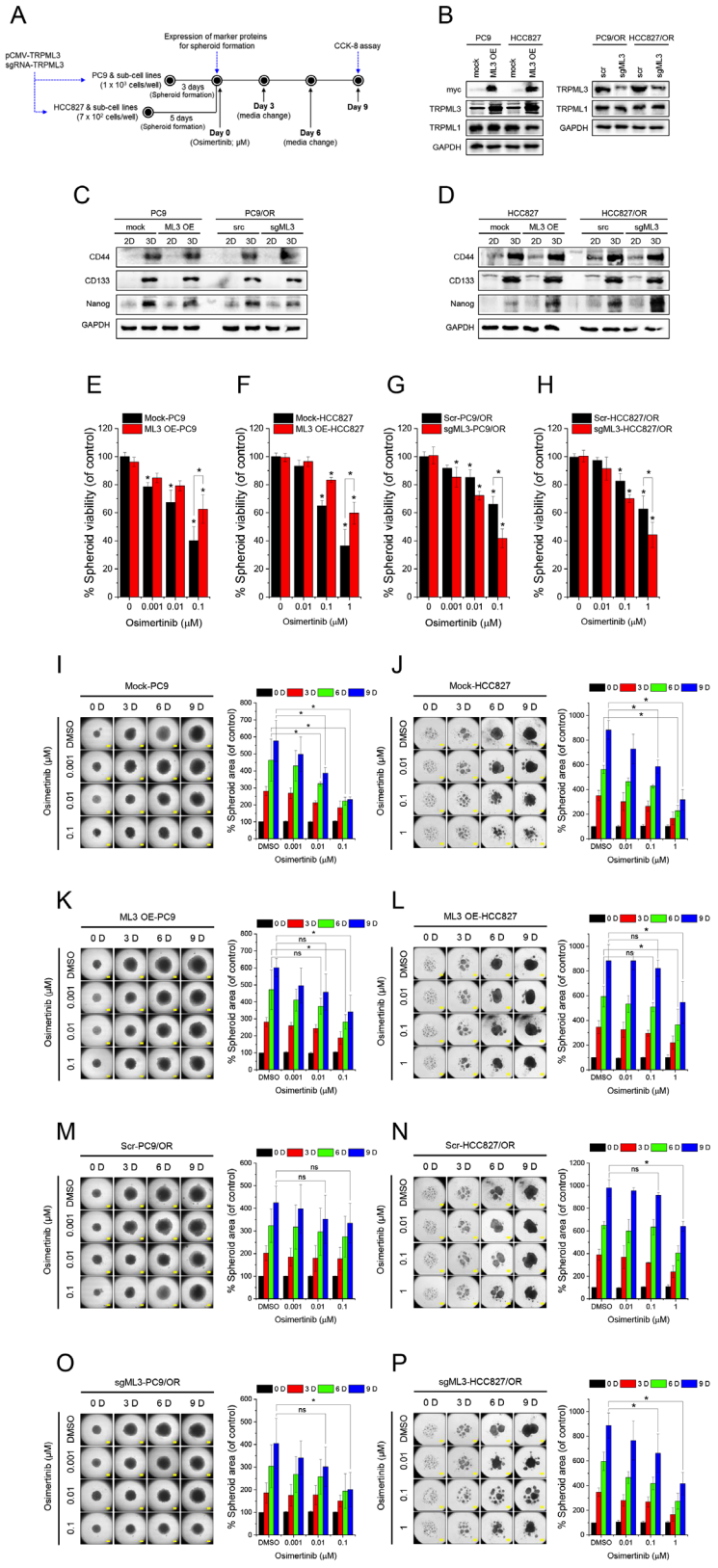

Figure 3. TRPML3 modulates osimertinib sensitivity and growth in spheroids. (A) Schematic representation of the spheroid formation protocol and the subsequent osimertinib treatment. (B) Expression levels of TRPML3 and -1 in PC9, HCC827 and their sublines (n=3). (C and D) Expression levels of spheroid formation markers, CD44, CD133 and Nanog in spheroid lysates from (C) PC9 and PC9/OR, (D) HCC827 and HCC827/OR, and conventional 2D cultures (2D). (E-H) Spheroid viability assessed using Cell Counting Kit-8 assays on day 9 of osimertinib treatment. Viability is expressed as percentage relative to corresponding DMSO-treated controls: (E) mock-PC9 and ML3 OE-PC9, (F) mock-HCC827 and ML3 OE-HCC827, (G) scr PC9/OR and sgML3-PC9/OR, (H) scr-HCC827/OR and sgML3-HCC827/OR. Data are shown as the mean ± SD (n=3). (I-P) Bright-field images of spheroids derived from mock-PC9 (I; n=3), mock-HCC827 (J; n=4), ML3 OE-PC9 (K; n=3), ML3 OE-HCC827 (L; n=4), scr-PC9/OR (M; n=3), scr-HCC827/OR (N; n=4), sgML3-PC9/OR (O; n=3), and sgML3-HCC827/OR (P; n=4) cells, captured at 3-day intervals following spheroid formation. Osimertinib treatment (DMSO, 0.001, 0.01, 0.1, and 1 μM) was initiated on day 0. Columns adjacent to each image show overall spheroid size relative to the control DMSO-treated spheroids on day 0. Data are presented as the mean ± SD. Scale bar, 400 μm. *P<0.05. TRPML, transient receptor potential mucolipin; ns, not significant.

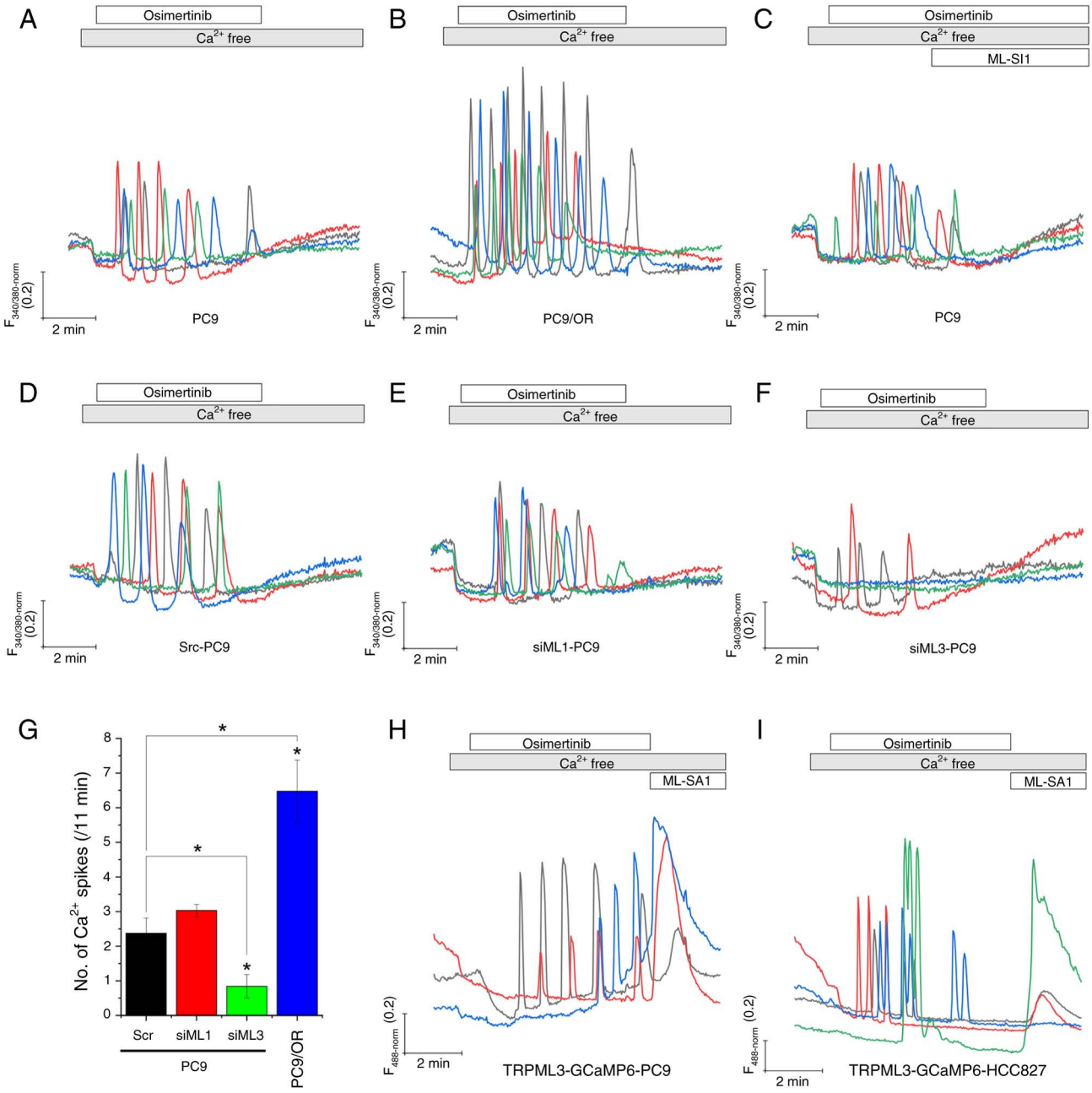

Figure 4. Osimertinib-induced $Ca^{2+}{}_i$ oscillations depend on lysosomal Ca^{2+} release mediated by TRPML3. $[Ca^{2+}]_i$ measured using Fura-2/AM in cells treated with 0.01 μM osimertinib in the absence of extracellular Ca^{2+}. (A and B) Osimertinib-induced $Ca^{2+}{}_i$ mobilization in (A) PC9 and (B) PC9/OR cells. (C) Effects of ML-SI1, a TRPML channel blocker, on osimertinib-induced $Ca^{2+}{}_i$ oscillations. (D-F) $Ca^{2+}{}_i$ oscillations in PC9 cells transfected with scrambled RNA (D; scr), TRPML1-targeting siRNA (E; siML1), or TRPML3-targeting siRNA (F; siML3), following osimertinib treatment. Each line represents $Ca^{2+}{}_i$ mobilization in a single cell. (G) Statistical analysis of Ca^{2+} spike frequencies ($^*P<0.05$, n=6). (H and I) Lysosomal Ca^{2+} release in (H) PC9 and (I) HCC827 cells expressing TRPML3-GCaMP6 and treated with 0.01 μM osimertinib in the absence of extracellular Ca^{2+}. ML-SA1 was used as a positive control. Lines indicate changes in GFP intensity (F_{488}) in individual cells, reflecting TRPML3-mediated lysosomal Ca^{2+} release. $F_{340/380}$ and F_{488} values were normalized to the mean and are presented as $F_{340/380\text{-norm}}$ and $F_{488\text{-norm}}$, respectively. TRPML, transient receptor potential mucolipin; si-, small interfering; scr, scrambled.

every 3 days until day 9. Those derived from PC9, HCC827 and their sublines continued to increase in size in the absence of osimertinib (Fig. 3I-P). By contrast, osimertinib treatment reduced spheroid size in both PC9 (Fig. 3I) and HCC827 (Fig. 3J) cells in a dose-dependent manner. Spheroids from TRPML3-overexpressing PC9 (Fig. 3K) and HCC827 (Fig. 3L) cells exhibited increased resistance to osimertinib, suppressing size reduction, whereas those derived from PC9/OR (Fig. 3M) and HCC827/OR (Fig. 3N) cells maintained their size even at higher osimertinib concentrations (0.01 and 0.1 μM for PC9/OR; 0.1 μM for HCC827/OR). TRPML3 silencing in PC9/OR (Fig. 3O) and HCC827/OR (Fig. 3P) cells restored osimertinib sensitivity, reducing spheroid size at 0.1 μM osimertinib.

TRPML3-mediated lysosomal Ca^{2+} release drives osimertinib-induced intracellular Ca^{2+} oscillations. To improve understanding of the TRPML3-mediated TKI resistance, it was determined whether TRPML3 channel activity contributed to osimertinib resistance by measuring $[Ca^{2+}]_i$.

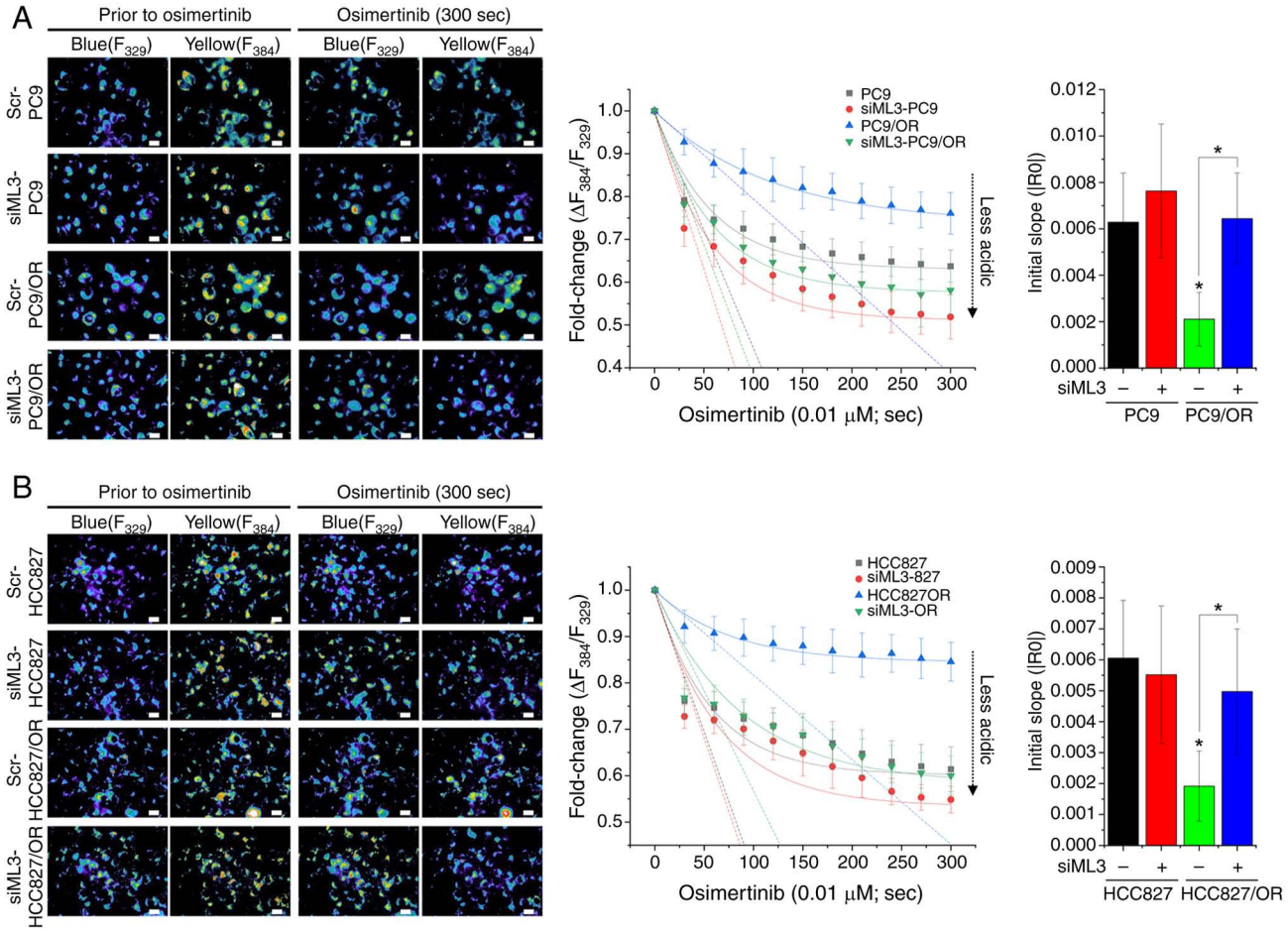

Figure 5. Osimertinib-induced lysosomal pH increase depends on TRPML3 levels. (A and B) Changes in PC9, PC9/OR, HCC827, and HCC827/OR cells. Initial fluorescence images were captured before exposing TRPML3-targeting siRNA (siML3) or scrambled RNA-transfected PC9 and PC9/OR (A) and HCC827 and HCC827/OR (B) cells to 0.01 μM osimertinib. Images were acquired every 30 sec, with fluorescence intensity quantified as F_{384}/F_{329}. Representative fluorescence images of F_{329} and F_{384} cells (left panel). Scale bar, 3 μm. Changes in lysosomal pH ($\Delta F_{384}/F_{329}$) relative to baseline (pre-osimertinib; mid-panel). Initial rates of pH increase (R0) are shown as the slope of each dotted line, with absolute values (|R0|) presented as the mean ± SD (right panel; n=3). *P<0.05. TRPML, transient receptor potential mucolipin; si-, small interfering; scr, scrambled.

Osimertinib treatment induced intracellular Ca^{2+} oscillations in PC9 cells, independently of extracellular Ca^{2+} (Fig. 4A). These oscillations were more pronounced in resistant PC9/OR cells (Fig. 4B) and were inhibited by ML-SI1, a mucolipin channel blocker (Fig. 4C). $Ca^{2+}{}_i$ oscillation frequency was significantly reduced in TRPML3-deficient cells but not in TRPML1-deficient cells (Fig. 4D-F). In TRPML3-deficient PC9 cells, Ca^{2+} spikes were significantly reduced, whereas PC9/OR cells with TRPML3 overexpression exhibited enhanced oscillations (Fig. 4G). To determine whether these oscillations depend on lysosomal Ca^{2+} release via TRPML3, the TRPML3-GCaMP6 construct was used. GFP fluorescence intensity closely mirrored the Fura-2 fluorescence pattern in osimertinib-treated cells, consistent with TRPML3-mediated lysosomal Ca^{2+} release (Fig. 4H and I).

TRPML3 knockdown enhances osimertinib-induced lysosomal pH increase. Lysosomal pH changes were next monitored using LysoSensor Yellow/Blue DND-160. The baseline fluorescence intensities were recorded before treatment, followed by continuous perfusion with HEPES buffer containing osimertinib. Osimertinib rapidly increased lysosomal pH in both PC9 (Fig. 5A) and HCC827 cells (Fig. 5B), reaching saturation at 60-65% of baseline. By contrast, osimertinib-resistant cells (PC9/OR and HCC827/OR) exhibited both a slower initial increase in lysosomal pH and a lower saturation level. TRPML3 deletion in osimertinib-resistant cells accelerated initial lysosomal pH elevation and increased its saturation level compared with that in scrambled control cells. These findings indicated that TRPML3 plays a critical role in the regulation of lysosomal pH changes induced by osimertinib in PC9 cells. Moreover, osimertinib-resistant NSCLC cells increased sequestration of osimertinib within lysosomes, a process that depends on TRPML3 expression. This suggests a link between TRPML3-mediated lysosomal Ca^{2+} release and regulation of lysosomal acidity.

TRPML3 deletion impairs osimertinib-induced TFEB nuclear translocation and lysosomal biogenesis. Building on the role of TRPML3 in lysosomal acidity regulation, it was determined whether it also plays a role in osimertinib-induced lysosomal biogenesis, which has been primarily associated with TPRML1. TFEB translocation from the cytosol to the nucleus was analyzed by fractionating total cellular proteins.

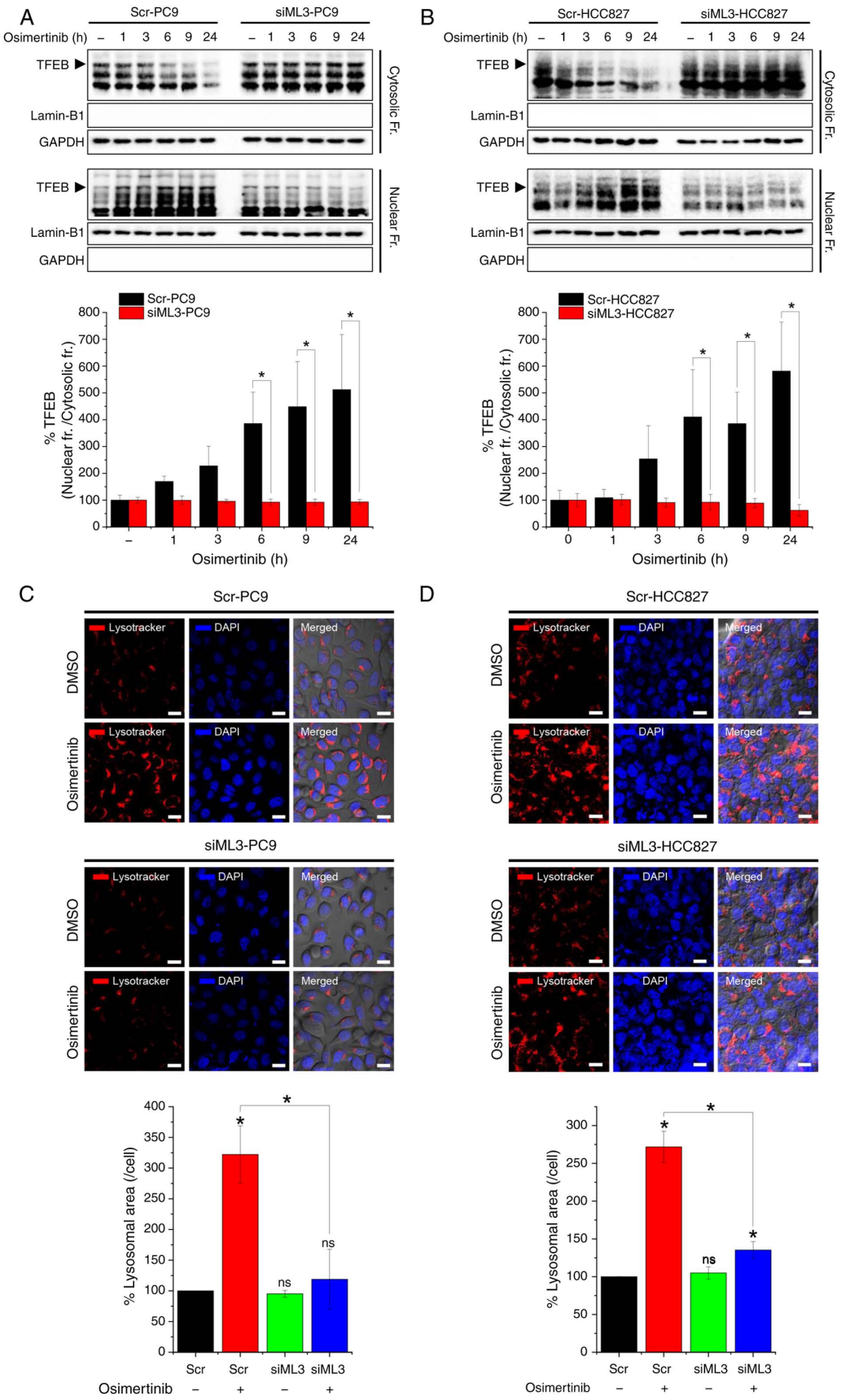

Figure 6. TRPML3 deficiency impairs osimertinib-induced lysosomal biogenesis. (A and B) TFEB levels in cytosolic and nuclear fractions of PC9 and HCC827 cells transfected with TRPML3-targeting siRNA (siML3) or scrambled RNA (control) and treated with 0.01 μM osimertinib for 1, 3, 6, 9, and 24 h. GAPDH and lamin-B1 served as cytosolic and nuclear markers, respectively. Quantitative analysis (lower panel) shows nuclear-to-cytosolic TFEB ratios expressed as percentages relative to control (scr-PC9 without osimertinib treatment; n=3). (C and D) Lysosomes and nuclei stained with LysoTracker Red DND-99 and DAPI after 24 h osimertinib treatment of cells transfected with siML3 or scr. Relative lysosomal area per cell is presented as a percentage of the control (scr-PC9 without osimertinib treatment; n=3). Scale bar, 20 μm. *P<0.05. TRPML, transient receptor potential mucolipin; si-, small interfering; scr, scrambled; ns, not significant.

Osimertinib increased the time-dependent nuclear translocation of TFEB in both PC9 (Fig. 6A) and HCC827 (Fig. 6B) cells. However, TRPML3 deletion completely blocked TFEB translocation. LysoTracker Red DND-99 staining revealed that the osimertinib-induced increase in lysosomal area was significantly reduced in TRPML3-deficient PC9 (Fig. 6C) and HCC827 (Fig. 6D) cells. In TRPML3-deficient cells, the lysosomal area was comparable to that in untreated control cells (scr-PC9 and scr-HCC827). These findings indicate that TRPML3 is essential for the regulation of TFEB nuclear translocation and lysosomal biogenesis in response to osimertinib-induced lysosomal pH alteration.

Discussion

Osimertinib (AZD9291) is a first-line TKI used to treat NSCLC with the T790M *EGFR* allele (30). Although initially effective, it often fails to prevent the emergence of residual tumors that become resistant over time (31). A known mechanism underlying this resistance involves the lysosomal sequestration of hydrophobic, weakly basic TKIs, such as gefitinib and osimertinib, which reduces TKI toxicity and promotes multi-drug resistance (32,33). However, the precise molecular mechanisms regulating this sequestration remain poorly understood. In the present study, lysosomal calcium channel TRPML3 (MCOLN3) was assessed as a potential contributor to TKI resistance. RNA expression analyses *EGFR*-mutant LUAD samples before and after osimertinib treatment, revealed that *TRPML3* expression was specifically increased in osimertinib-residual tumors, unlike TRPML1 and -2, suggesting a distinct role for TRPML3 in mediating drug resistance. It was demonstrated that osimertinib-induced increases in $[Ca^{2+}]_i$ levels depend on TRPML3-mediated lysosomal Ca^{2+} release, which is critical for maintaining lysosomal acidity. Furthermore, TRPML3, rather than TRPML1, was found to be crucial for lysosomal biogenesis through Ca^{2+}-dependent TFEB activation in osimertinib-treated NSCLC cells. Experiments using NSCLC-derived spheroids further confirmed that modulating *TRPML3* expression alters osimertinib sensitivity, underscoring TRPML3 as a potential therapeutic target to overcome drug resistance in NSCLC.

Several studies have addressed the role of TRPML1 in lysosomal signaling and autophagy; however, it remains less characterized in cancer biology. The Cancer Genome Atlas data show that TRPML3 expression is decreased in multiple cancers, including LUAD (34). Our data provide the first evidence, to the best of our knowledge, that increased TRPML3 expression in residual tumors following osimertinib treatment contributes to drug resistance.

As an inward-rectifying cation channel (35), TRPML3 has been implicated in autophagy, particularly in autophagosome biogenesis during endocytosis and phagocytosis (17,36). Autophagy plays a dual role in cancer, as it prevents tumor initiation by mitigating cellular stress but supports tumor progression by sustaining proliferation and metabolic activity (37). Although the relationship between TRPML3 and autophagy was not fully explored, they suggest that TRPML3-mediated enhancement of autophagic flux in osimertinib-resistant contributes to drug resistance. Key limitations of the present study include the absence of *in vivo* validation and the lack of direct investigation into the interaction between TRPML3 and autophagy in the context of TKI resistance. Given the established involvement of TRPML3 in autophagy (17,36), future studies should determine whether TRPML3-driven lysosomal Ca^{2+} signaling enhances autophagy-mediated drug sequestration. To this end, important future directions include monitoring autophagic flux in NSCLC cells in response to changes in TRPML3 expression and evaluating whether co-targeting TRPML3 and autophagy enhances the efficacy of osimertinib *in vivo*. Clarifying the relationship between TRPML3 and autophagy will deepen our understanding of resistance mechanisms and guide the development of combination therapies.

Our study underscores the critical role of TRPML3 in regulating the lysosomal sequestration of TKIs and promoting lysosomal biogenesis in NSCLC cells. Previously, the authors identified TRPML3 as a key contributor to drug resistance and demonstrated that lysosomal Ca^{2+} release via TRPML3 facilitates lysosomal trafficking to the plasma membrane, enhancing resistance. This mechanism is influenced by gefitinib-induced lysosomal pH changes, as gefitinib is a lysosomotropic weak base (38). Emerging evidence suggests that lysosomal Ca^{2+} release mediated by TRPML3 is essential for maintaining lysosomal acidification, as Ca^{2+} efflux is coupled with H^+ uptake into the lumen (20,39-41). Given that this acidification drives lysosomotropic agent sequestration, TRPML3 likely enhances sequestration by preserving the lysosomal proton gradient. Based on these studies, it was hypothesized that TKI sequestration elevates lysosomal pH, which in turn triggers lysosomal Ca^{2+} release via TRPML3 but not TRPML1. This Ca^{2+} release is coupled with increased H^+ uptake, further enhancing sequestration. The present findings support this hypothesis: osimertinib treatment rapidly increased lysosomal pH; moreover, the rate of pH increase was directly correlated with TRPML3 expression. Additionally, osimertinib-induced Ca^{2+} mobilization depends on TRPML3-mediated lysosomal Ca^{2+} release. These findings suggest that osimertinib resistance is enhanced in NSCLC cells by increasing the lysosomal sequestration of TKIs. By elucidating the role of TRPML3 in these processes, the present study provides valuable insights into drug resistance mechanisms and identifies potential therapeutic targets.

It was observed that osimertinib-induced lysosomal pH elevation does not favor TRPML1 activation, as TRPML1 functions optimally in a more acidic environment. Prolonged TKI treatment increases both lysosomal number and size (33,42). While TRPML1 is well known for its role in lysosomal biogenesis through Ca^{2+} release and TFEB dephosphorylation (13), the mechanism by which weak-base chemotherapeutics such as osimertinib induce lysosomal Ca^{2+} release remains unclear. Given that TRPML3 is activated at higher pH, it was hypothesized that it compensates for TRPML1 by activating TFEB and promoting lysosomal biogenesis. Consistent with this, it was observed that TRPML3 depletion inhibited TFEB nuclear translocation and reduced osimertinib-induced lysosomal biogenesis. These results provide new insights into lysosomal regulation in cancer cells treated with TKIs such as osimertinib. Further studies are needed to elucidate the molecular pathways involved and evaluate the therapeutic potential of targeting TRPML channels in cancer treatment.

In conclusion, a novel mechanism was identified, by which TRPML3 contributes to osimertinib resistance in NSCLC by regulating lysosomal biogenesis and function. Our results suggest a compensatory relationship between TRPML3 and TRPML1 in response to TKI-induced lysosomal changes. By identifying TRPML3 as a key regulator, the present study provides new insights into the molecular basis of drug resistance and highlights TRPML3 as a promising therapeutic target.

Acknowledgements

The authors would like to thank Dr Jin Kyung Rho (Asan Medical Center, Ulsan University) and Dr Hyun Jin Kim (Sungkyunkwan University) for providing NSCLC cell lines and GCaMP-TRPML3 plasmid constructs, respectively.

Funding

The present study was supported by the National Research Foundation of Korea and funded by the Ministry of Education (grant no. RS-2023-NR076426).

Availability of data and materials

The data generated in the present study are included in the figures of this article. The data generated in the present study may be requested from the corresponding author.

Authors' contributions

MSeoK contributed to data curation, formal analysis, investigation, methodology, software, and wrote the initial draft. MSeuK was responsible for conceptualization, formal analysis, funding acquisition, investigation, project administration, supervision, validation, and editing the manuscript. Both authors read and approved the final version of the manuscript and confirm the authenticity of all the raw data.

Ethics approval and consent to participate

Not applicable.

Patient consent for publication

Not applicable.

Competing interests

The authors declare that they have no competing interests.

References

1. Zhang Z, Yue P, Lu T, Wang Y, Wei Y and Wei X: Role of lysosomes in physiological activities, diseases, and therapy. J Hematol Oncol 14: 79, 2021.
2. Savini M, Zhao Q and Wang MC: Lysosomes: Signaling hubs for metabolic sensing and longevity. Trends Cell Biol 29: 876-887, 2019.
3. Hraběta J, Belhajová M, Šubrtová H, Merlos Rodrigo MA, Heger Z and Eckschlager T: Drug sequestration in lysosomes as one of the mechanisms of chemoresistance of cancer cells and the possibilities of its inhibition. Int J Mol Sci 21: 4392, 2020.
4. Yamagishi T, Sahni S, Sharp DM, Arvind A, Jansson PJ and Richardson DR: P-glycoprotein mediates drug resistance via a novel mechanism involving lysosomal sequestration. J Biol Chem 288: 31761-31771, 2013.
5. Seebacher N, Lane DJ, Richardson DR and Jansson PJ: Turning the gun on cancer: Utilizing lysosomal P-glycoprotein as a new strategy to overcome multi-drug resistance. Free Radic Biol Med 96: 432-445, 2016.
6. Zhitomirsky B and Assaraf YG: Lysosomes as mediators of drug resistance in cancer. Drug Resist Updat 24: 23-33, 2016.
7. Xu H and Ren D: Lysosomal physiology. Annu Rev Physiol 77: 57-80, 2015.
8. Kendall RL and Holian A: The role of lysosomal ion channels in lysosome dysfunction. Inhal Toxicol 33: 41-54, 2021.
9. Xu M and Dong XP: Endolysosomal TRPMLs in cancer. Biomolecules 11: 65, 2021.
10. Bargal R, Avidan N, Ben-Asher E, Olender Z, Zeigler M, Frumkin A, Raas-Rothschild A, Glusman G, Lancet D and Bach G: Identification of the gene causing mucolipidosis type IV. Nat Genet 26: 118-123, 2000.
11. Santoni G, Maggi F, Amantini C, Marinelli O, Nabissi M and Morelli MB: Pathophysiological role of transient receptor potential mucolipin channel 1 in calcium-mediated stress-induced neurodegenerative diseases. Front Physiol 11: 251, 2020.
12. Soyombo AA, Tjon-Kon-Sang S, Rbaibi Y, Bashllari E, Bisceglia J, Muallem S and Kiselyov K: TRP-ML1 regulates lysosomal pH and acidic lysosomal lipid hydrolytic activity. J Biol Chem 281: 7294-7301, 2006.
13. Di Paola S, Scotto-Rosato A and Medina DL: TRPML1: The $Ca^{(2+)}$retaker of the lysosome. Cell Calcium 69: 112-121, 2018.
14. Qi J, Li Q, Xin T, Lu Q, Lin J, Zhang Y, Luo H, Zhang F, Xing Y, Wang W, *et al*: MCOLN1/TRPML1 in the lysosome: A promising target for autophagy modulation in diverse diseases. Autophagy 20: 1712-1722, 2024.
15. Medina DL, Di Paola S, Peluso I, Armani A, De Stefani D, Venditti R, Montefusco S, Scotto-Rosato A, Prezioso C, Forrester A, *et al*: Lysosomal calcium signalling regulates autophagy through calcineurin and TFEB. Nat Cell Biol 17: 288-299, 2015.
16. Kim SW, Kim DH, Park KS, Kim MK, Park YM, Muallem S, So I and Kim HJ: Palmitoylation controls trafficking of the intracellular Ca^{2+} channel MCOLN3/TRPML3 to regulate autophagy. Autophagy 15: 327-340, 2019.
17. Kim SW, Kim MK, Hong S, Choi A, Choi JH, Muallem S, So I, Yang D and Kim HJ: The intracellular Ca^{2+} channel TRPML3 is a PI3P effector that regulates autophagosome biogenesis. Proc Natl Acad Sci USA 119: e2200085119, 2022.
18. Paroutis P, Touret N and Grinstein S: The pH of the secretory pathway: Measurement, determinants, and regulation. Physiology (Bethesda) 19: 207-215, 2004.
19. Miao Y, Li G, Zhang X, Xu H and Abraham SN: A TRP channel senses lysosome neutralization by pathogens to trigger their expulsion. Cell 161: 1306-1319, 2015.
20. Gerasimenko JV, Tepikin AV, Petersen OH and Gerasimenko OV: Calcium uptake via endocytosis with rapid release from acidifying endosomes. Curr Biol 8: 1335-1338, 1998.
21. Martina JA, Lelouvier B and Puertollano R: The calcium channel mucolipin-3 is a novel regulator of trafficking along the endosomal pathway. Traffic 10: 1143-1156, 2009.
22. Liang J, Bi G, Sui Q, Zhao G, Zhang H, Bian Y, Chen Z, Huang Y, Xi J, Shi Y, *et al*: Transcription factor ZNF263 enhances EGFR-targeted therapeutic response and reduces residual disease in lung adenocarcinoma. Cell Rep 43: 113771, 2024.
23. Chen S, Zhou Y, Chen Y and Gu J: fastp: An ultra-fast all-in-one FASTQ preprocessor. Bioinformatics 34: i884-i890, 2018.
24. Dobin A, Davis CA, Schlesinger F, Drenkow J, Zaleski C, Jha S, Batut P, Chaisson M and Gingeras TR: STAR: Ultrafast universal RNA-seq aligner. Bioinformatics 29: 15-21, 2013.
25. Patro R, Duggal G, Love MI, Irizarry RA and Kingsford C: Salmon provides fast and bias-aware quantification of transcript expression. Nat Methods 14: 417-419, 2017.
26. Robinson MD, McCarthy DJ and Smyth GK: edgeR: A Bioconductor package for differential expression analysis of digital gene expression data. Bioinformatics 26: 139-140, 2010.
27. Chu VT, Gottardo R, Raftery AE, Bumgarner RE and Yeung KY: MeV+R: Using MeV as a graphical user interface for Bioconductor applications in microarray analysis. Genome Biol 9: R118, 2008.
28. Livak KJ and Schmittgen TD: Analysis of relative gene expression data using real-time quantitative PCR and the 2(-Delta Delta C(T)) method. Methods 25: 402-408, 2001.

29. Kurien BT and Scofield RH: Western blotting: An introduction. Methods Mol Biol 1312: 17-30, 2015.
30. Ramalingam SS, Vansteenkiste J, Planchard D, Cho BC, Gray JE, Ohe Y, Zhou C, Reungwetwattana T, Cheng Y, Chewaskulyong B, *et al*: Overall survival with osimertinib in untreated, EGFR-mutated advanced NSCLC. N Engl J Med 382: 41-50, 2020.
31. Ohashi K, Maruvka YE, Michor F and Pao W: Epidermal growth factor receptor tyrosine kinase inhibitor-resistant disease. J Clin Oncol 31: 1070-1080, 2013.
32. Halaby R: Influence of lysosomal sequestration on multidrug resistance in cancer cells. Cancer Drug Resist 2: 31-42, 2019.
33. Zhitomirsky B and Assaraf YG: Lysosomal sequestration of hydrophobic weak base chemotherapeutics triggers lysosomal biogenesis and lysosome-dependent cancer multidrug resistance. Oncotarget 6: 1143-1156, 2015.
34. Wu M, Li X, Zhang T, Liu Z and Zhao Y: Identification of a nine-gene signature and establishment of a prognostic nomogram predicting overall survival of pancreatic cancer. Front Oncol 9: 996, 2019.
35. Kim HJ, Li Q, Tjon-Kon-Sang S, So I, Kiselyov K and Muallem S: Gain-of-function mutation in TRPML3 causes the mouse Varitint-Waddler phenotype. J Biol Chem 282: 36138-36142, 2007.
36. Kim HJ, Soyombo AA, Tjon-Kon-Sang S, So I and Muallem S: The Ca(2+) channel TRPML3 regulates membrane trafficking and autophagy. Traffic 10: 1157-1167, 2009.
37. Debnath J, Gammoh N and Ryan KM: Autophagy and autophagy-related pathways in cancer. Nat Rev Mol Cell Biol 24: 560-575, 2023.
38. Kim MS, Yang SH and Kim MS: TRPML3 enhances drug resistance in non-small cell lung cancer cells by promoting Ca^{2+}-mediated lysosomal trafficking. Biochem Biophys Res Commun 627: 152-159, 2022.
39. Christensen KA, Myers JT and Swanson JA: pH-dependent regulation of lysosomal calcium in macrophages. J Cell Sci 115: 599-607, 2002.
40. Morgan AJ, Platt FM, Lloyd-Evans E and Galione A: Molecular mechanisms of endolysosomal Ca2+ signalling in health and disease. Biochem J 439: 349-374, 2011.
41. Shen D, Wang X, Li X, Zhang X, Yao Z, Dibble S, Dong XP, Yu T, Lieberman AP, Showalter HD and Xu H: Lipid storage disorders block lysosomal trafficking by inhibiting a TRP channel and lysosomal calcium release. Nat Commun 3: 731, 2012.
42. de Araujo MEG, Liebscher G, Hess MW and Huber LA: Lysosomal size matters. Traffic 21: 60-75, 2020.